

# Experiments on gravity currents propagating down slopes. Part 2. The evolution of a fixed volume of fluid released from closed locks into a long, open channel

T. MAXWORTHY†

Department of Aerospace and Mechanical Engineering, University of Southern California,  
Los Angeles, CA 98009-1191, USA

(Received 2 June 2008 and in revised form 12 January 2009)

A series of experiments have been carried out on gravity currents released from locks of various dimensions into a sloping, open channel. Initially all the driving heads of the gravity currents grew by addition of heavier material from a following down-slope flow and by entrainment of ambient fluid, as in Maxworthy & Nokes (*J. Fluid Mech.*, vol. 584, 2007, pp. 433–453). After propagating a distance of the order of 5–10 lock lengths the inflow into the rear stopped, and the head began to lose buoyancy-containing fluid from its rear by the detachment of large, weakly vortical structures. At the same time it was still entraining fluid over the majority of its surface so that its mean density was reduced. Measurements using a semi-direct method, in which dye concentration was used as a surrogate for density, have shown that the buoyancy in the current head increased during the first phase and decreased during the second. At no stage was the buoyancy constant except, of course, at the location and time at which the buoyancy was maximum with a magnitude significantly smaller than the initial value in the lock. Despite this the constant buoyancy theory of Beghin, Hopfinger & Britter (*J. Fluid Mech.*, vol. 107, 1981, pp. 407–422), in which the head location  $x$  varies with time  $t$  as  $t^{2/3}$  during the later velocity-decay stage of the evolution, was found to be remarkably robust as a description of the evolution over both the latter part of the increasing-buoyancy stage and all of the decreasing-buoyancy phase. Critically, however, the multiplying coefficient had to be smaller than presented by them in order to track the experimental data with precision. This was due principally to the observation that the buoyancy at the beginning of the decay phase was considerably smaller than the initial buoyancy in the lock.

---

## 1. Introduction

This paper is a continuation of the experiments and analysis of Maxworthy & Nokes (2007) but in a longer, sloping channel fitted with enclosed locks of different dimensions, i.e. ones with various depths and lengths fitted with a solid upper lid, that were completely filled with dense fluid as in Maxworthy & Nokes (2007). In all cases the interior of the channel was open to a deep ambient fluid; i.e. there was no solid top to the channel, and the growth of the current head was not constrained by presence of a top wall as in the case of a closed channel. In this case the emphasis is mainly, but not exclusively, on the evolution of the current at later times, after the

† Email address for correspondence: maxworth@usc.edu

head had reached its maximum buoyancy and was, in fact, losing buoyancy. This is in contrast to Maxworthy & Nokes (2007), where the emphasis was on the initial filling of the head with dense fluid. As a result it is possible to make statements about the further relevance of the theory of Beghin *et al.* (1981). In this regime the Beghin *et al.* (1981) theory reduces to a very simple result that can also be found by trivial dimensional arguments, the details of which are shown in §3. This formulation was then used to examine a wide range of experimental circumstances and to unravel a number of the physical processes that were at work in this simple geometry.

The environmentally important problem of gravity current (GC) motion over a horizontal surface has received an enormous amount of attention. Probably the first location to look for information on the subject is the research monograph of Simpson (1987) which reviews a wide range of possible cases. There are countless research papers covering an even wider range of problems, and reference will be made to the most appropriate and useful ones in what follows. However, for the problem at hand, the motion of GCs down slopes, the literature is much less extensive. In fact only a handful of works come immediately to mind. Consider first the work of Britter & Linden (1980) which considers the case of a constant flow rate of heavy fluid down slopes at angles to the horizontal ( $\theta$ ) varying from  $5^\circ$  to  $90^\circ$ . In the theory they presented they made use of experiments by Ellison & Turner (1959) on turbulent entrainment into a steady, constant flow-rate density current flowing down a slope and used it to estimate the flow rate into the head of the current and hence its velocity. While this work has some relevance to the present effort which is, in essence, an unsteady version of their argument it is experiments by the LEGI group at the IMG of the University of Grenoble and collaborators on the release of a fixed volume of dense fluid that is used in what follows. The major interest of the LEGI group was in the dynamics of powder-snow avalanches, starting with Hopfinger & Tochon-Danguy (1977) and Tochon-Danguy (1977) and continuing with Beghin *et al.* (1981), Laval *et al.* (1988) and Rastello & Hopfinger (2004). Since some of these items are to be considered in detail in the theory and discussion sections of this paper most details are postponed until that time. In summary, their experiments showed that a constant volume release gave a front velocity that first increased and then decreased as the square root of distance from a virtual source. However, in Maxworthy & Nokes (2007) the velocity always increased to a maximum at a distance from the lock that was considerably larger than that predicted by the theory. This apparent discrepancy was explained by the observation that the head was being fed over a considerable distance by a following or feeding current from the main volume in the lock. This information was then used to modify the theory of Beghin *et al.* (1981). The results of Laval *et al.* (1988) are similar except they use a much larger initial volume/unit width ( $400\text{--}500\text{ cm}^2$ ) than used here and in the LEGI experiments. Other studies that are tangentially related to the present work are those of Alavian (1986) who looked at three-dimensional sources, Liu, Schlapfer & Buhler (1991) with a concentration on very small slopes and Luthi (1981) and Kersey & Hsu (1976) who added surface friction to the Beghin *et al.* (1981) formulation as did Rastello & Hopfinger (2000) who also studied the entrainment of particles from an erodable bed and non-Boussinesq effects. Further studies include those of Webber, Jones & Martin (1993) and Tickle (1996) who considered the evolution of a *wedge*-shaped cloud on a slope with and without entrainment respectively, while the latter also considered the case of a two-dimensional current.

A recent numerical study of the lock-exchange problem in an enclosed channel on a slope, i.e. where the lock region and test region have equal lengths and where the

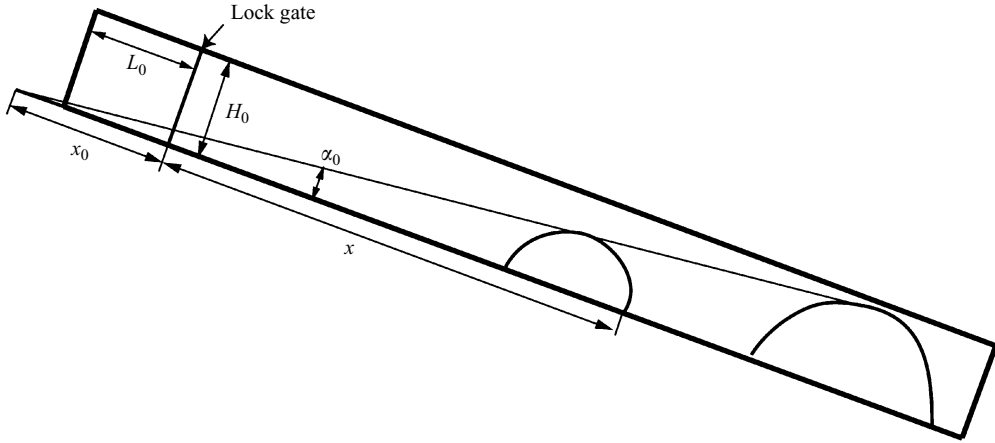


FIGURE 1. Unscaled sketch of the test channel, showing the closed lock ( $L_0 \times H_0$ ) and the current head at two locations at different times late in the motion. The line joining their maximum heights defines the angle of growth ( $\alpha_0$ ) and its intersection with the channel base the virtual origin, at  $-x_0$ , for the decaying phase of the current head evolution. The angle of the channel to the horizontal is designated as  $\theta$ .

---

	$L_0 = 20$ cm	$L_0 = 10$ cm	$L_0 = 5.5$ cm
$H_0 = 10$ cm	6; 3	4; 4	6; 3
$H_0 = 5$ cm	–	5; 3	8; 5
$H_0 = 2.5$ cm	–	–	8; 5

---

TABLE 1. Closed lock. Channel slopes to the horizontal ( $\theta$ )  $10.6^\circ$  and  $5.9^\circ$ . The numbers in each group indicate the number of experiments performed at  $10.6^\circ$  and  $5.9^\circ$  respectively. Typically the range of  $g'_0$  in any one of these sequences was between 12 and  $120 \text{ cm s}^{-2}$ .

---

top of the channel is closed, has been published by Birman *et al.* (2007). In this case the two-dimensional numerical simulations give a head velocity that rises rapidly to a constant velocity that lasts for about 10 lock heights and then enters an unsteady phase. In agreement with Maxworthy & Nokes (2007) they also found a feeding current from the main volume of the lock contents that maintained a high head velocity. However, the differences in geometry resulted in substantial, quantitative differences between the two studies.

## 2. Apparatus and experimental procedure

The channel used in these experiments was manufactured with a running length of 230 cm, width 15.2 cm and height 10 cm. The lock was constructed with three different lengths ( $L_0$ ) of nominal values 20 cm, 10 cm or 5 cm with a wall added to its top and a lock gate to initially enclose it completely, i.e. a closed lock, as in the experiments of Maxworthy & Nokes (2007). Various values of lock height,  $H_0$ , were used also. A sketch of the apparatus is shown in figure 1 together with the definitions of the items of interest. All operating conditions are summarized in table 1.

The initial buoyancy/unit width ( $B_0$ ) in the lock was  $B_0 = g'_0 L_0 H_0$ , where  $g'_0 = g(\rho_C - \rho_0)/\rho_0$ ;  $\rho_C$  is the density of the fluid in the lock;  $\rho_0$  is the density of the ambient; and  $g$  is the acceleration of gravity. The channel was placed in a water-filled

tank that was 244 cm long, 75 cm wide and 65 cm deep and the free surface of which was 10 cm above the upper edge of the lock gate in experiments at a slope angle of  $\theta = 5.9^\circ$  and 5 cm at the maximum possible angle of  $10.6^\circ$ . Because of the limiting height of the tank it was not possible to study angles larger than these even though such a study would have been very desirable; it is therefore left to future experiments when a deeper tank can be located. As before the diagnostic measures considered were the  $x$  versus  $t$  trajectories of the GC head, together with plots of  $(x + x_0)^{3/2}$  versus  $t$  that revealed deviations from the theoretical formulation. The reason for the latter scaling is discussed in detail in §3. Here  $x$  and  $t$  are the location and time of the nose of the current from the lock gate respectively and  $x_0$  the distance from the virtual origin of the motion to the lock gate as shown in figure 1.

When the qualitative observations of previous workers was confirmed, i.e. that there was a substantial loss of buoyancy from the GC head during its nominally constant buoyancy phase, it was decided that a more direct measure of the loss was needed than the indirect method discussed in §3. In this technique dye was used as a surrogate for density as in Cenedese & Dalziel (1998), for example. Using a Sony video camera, with a 3.0 megapixel CCD array, full-frame photographs of the GC head were taken in two modes. First was a calibration mode: here photographs were taken of acrylic cells, of the same material and width as the test channel, filled with salt solutions of known density and linearly related dye concentrations. These were analysed using the Adobe Photoshop CS3 histogram function to determine the average luminance or intensity of both the sample ( $L_C$ ) and background ( $L_B$ ) under uniform back-lighting conditions. Then the quantity  $L_R = (L_B - L_C)/L_B$  could be related to  $(\rho_C - \rho_0)/\rho_0$ , where  $\rho_C$  was the known sample density and  $\rho_0$  the known background density of pure water. The resulting calibration function was very nonlinear; however most of the present measurements were taken in a regime in which the calibration was close to linear so that inaccuracies due to the nonlinearity were minimized. This procedure was repeated with the camera mounted on a moving carriage which was in turn placed on a track angled at the same value as the channel itself and with the same backlighting as the calibration test. Individual still images were extracted from the video tapes and imported into Photoshop CS3. Then, using the lasso and histogram functions, both the average value of  $L_R$  over the area of the evolving head and the area itself could be determined to calculate the buoyancy residing in it at each instant a photograph was taken. Here, the main reason for any measurement inaccuracy was the difficulty in deciding the rearward boundary of the head. During the initial phase of the motion, when buoyancy was still entering the head, this was relatively straightforward, since the boundary was quite clearly marked by the trailing limit of the recirculation zone, as in Maxworthy & Nokes (2007). Later, once substantial shedding of buoyancy took place, in the form of large, dyed vortices that followed and moved slower than the main head, the demarcation was harder to see, and one had to rely on viewing the video in real time to see where the dyed, heavier fluid was being recirculated at the rear of the head. This difficulty can be seen on viewing any of the photographic sequences that follow in §4 and by study of the sketches of figure 3 which attempt to remove some of the ambiguity inherent in this process. Many of the images were analysed several times and in different ways, e.g. by dividing the image into multiple areas of differing uniform luminosity, i.e. the areas between contours of constant luminosity, in order to obtain statistics on the errors involved. In this way an overall error bar of  $\pm 10\%$  was assigned to the measurements. The uncertainty can be seen also as an increase in data scatter at later times in the plots in the resultant data.

### 3. Theoretical preamble and preliminary discussion of the experiments

As a consequence of the results of Maxworthy & Nokes (2007), in which it was found that a closed lock with the dimensions 20 cm  $\times$  10 cm resulted in an initial evolution that could only be explained by a theory with increasing head buoyancy, it was decided to run a series of experiments with locks with various different values of  $L_0$  and  $H_0$  but in a longer channel as discussed in §2. In the majority of this paper the desire is to explore conditions that lead to a possible GC evolution that more closely resembles the one with constant buoyancy at the later stages of the motion.

As before the distance of the front of the current,  $x$ , from the lock gate was measured as a function of time,  $t$ , from its opening. In order to most readily determine the predicted scaling for the position history both the raw data, i.e.  $x$  versus  $t$  and its derivative  $U$  versus  $x$  or  $t$ , were plotted. In order to emphasize the predicted  $t^{2/3}$  behaviour for  $x$  during the decay phase, as determined from Beghin *et al.* (1981) and dimensional arguments for ‘constant buoyancy’,  $(x + x_0)^{3/2}$  versus  $t$ , was plotted, i.e. taking the 3/2 power of (3.1). Here  $x_0$ , as in Maxworthy & Nokes (2007), is the distance between the location of the virtual origin and, in this case, the lock gate. This quantity was determined by extrapolation to the bottom of the channel from estimates of the spreading angle of the maximum height of the head ( $\alpha_0$ ) of the current over the decaying portion of the velocity history, as shown in figure 1 and tabulated in table 2(a) in §5. Thus, the measured slope  $K$  of the plots of  $(x + x_0)^{3/2}$  versus  $t$ , if constant over a significant range of  $x$  and  $t$ , should give one dimensionless measure of the decay. Then the time from the virtual origin  $t_0$  could be found by extrapolation. The estimate of  $x_0$  given above was used as a first guess, while values both slightly larger and smaller were also used to give a realistic range of values of the constant of proportionality ( $K_M$ ) in the equation

$$(x + x_0) = K_M B_0^{1/3} (t + t_0)^{2/3}, \quad (3.1)$$

where  $K_M = K^{2/3} / B_0^{1/3}$  is a quantity that one might expect to be constant at any given value of  $\theta$ . As mentioned above, the present experiments show that this is not so and that the geometry of the lock and variations from experiment to experiment also play a role.

It seems natural to present the results in dimensionless form, but one can argue that that, in a sense, (3.1) is already dimensionless. This can be rationalized as follows: Note that  $B_0 = A_0 g_0'$ , where  $A_0 = L_0 H_0$ . Hence  $B_0^{1/3} = A_0^{1/2} (g_0'^{1/3} / A_0^{1/6})$ . Then (3.1) can be written exactly as

$$(x + x_0) / A_0^{1/2} = K_M [(t + t_0) / (A_0^{1/4} / g_0'^{1/2})]^{2/3}. \quad (3.2)$$

From this it is clear that the most important dimensionless quantity to be determined from the experiments is  $K_M$ , since it is a measure of the non-universality of the scaling from experiment to experiment. At the same time the dimensionless quantities determining the location of the virtual origin can be tabulated (see table 2b in §5) as  $x_0 / A_0^{1/2}$  and  $t_0 / (A_0^{1/4} / g_0'^{1/2})$ . All three should be independent of  $B_0$  and only depend on the channel slope,  $\theta$ , and the lock aspect ratio,  $L_0 / H_0$ . However, the detailed results suggest that this simple suggestion needs to be supplemented by some new and, as yet, unknown proposal. In what follows the raw data is used to determine  $K_M$ ,  $x_0$  and  $t_0$ , while the appropriate dimensionless values are to be found in table 2(a, b) in §5.

By differentiating (3.1) the velocity of the front ( $U$ ) is given by  $U = dx/dt = (2K_M/3) B_0^{1/3} (t + t_0)^{-1/3}$ , with  $B_0$  initially assumed to be a known independent quantity.

In this case  $U$  can be made dimensionless using the independent velocity scale  $A_0^{1/4} g_0^{1/2}$ .

Over the wide range of experiments that were performed it was found that the behaviour of current obeyed the prescription given above, based on the simplest dimensional arguments, in an approximate sense. In fact, variations with exponents slightly numerically smaller than  $2/3$  gave a better statistical fit to the data, although the  $t^{2/3}$  result was considered to be a very good first approximation under most conditions. Also, a scaling with  $B_0^{1/3}$  did not result in a universal multiplicative constant,  $K_M$ , at a given angle and aspect ratio as might be expected, although it is not unreasonable to use an average value under appropriate circumstances as discussed in §5. It is proposed that these latter effects were firstly the result of incomplete capture of the buoyancy in the initial lock charge that varied somewhat from experiment to experiment, as in Maxworthy & Nokes (2007), and subsequent removal of buoyancy from the driving head of the current. That is once the head had gained its maximum buoyancy from the following current, which was invariably less than the full value, as discussed in detail in Maxworthy & Nokes (2007), it did not propagate with that value but with a value that was continuously decreasing. Somewhat surprisingly, as shown later, these effects could not be captured entirely by the expected dependence on lock aspect ratio at a given slope. To show this test sequences were run with the values of  $L_0$  and  $H_0$  given in table 1 for closed locks to determine under what circumstances any given history was followed. This was quantified by (i) comparing with the gain and subsequent loss of  $B$  measured directly using the quantitative photographic method detailed in §2 and (ii) a comparison of the measured value of  $K_M$  with the equivalent value  $K_B$  from the Beghin *et al.* (1981) theory. The first technique is discussed in §2, while the second is discussed below.

### 3.1. Use of the Beghin *et al.* (1981) theory to estimate buoyancy loss when $x$ nominally varies as $t^{2/3}$ .

From the theory of Beghin *et al.* (1981) one can quantify the loss of buoyancy in some averaged sense during the later part of the head evolution. That theory can be cast in a form that allows direct comparison with the experimental measurements. Thus the decay law can be written as

$$(x + x_0) = K_B B_0^{1/3} (t + t_0)^{2/3}, \quad (3.3)$$

where  $K_B$  is the theoretical equivalent of the experimentally measured quantity  $K_M$ . Then from the Beghin *et al.* (1981) theory

$$K_B = 1.333 [1 + 0.449(1 + k^2)^{1/2} \alpha_0/k] [k \sin \theta / \alpha_0^2 (1 + 4k^2)(1 + 2k)]^{1/3}, \quad (3.4)$$

where  $k = H/L$  in which  $H$  is the local height and  $L$  the local length of the head, and the term  $[B/B_0]^{1/3}$  has been removed so that it can be calculated by comparing the measured value of  $K_M$  with the theoretical value  $K_B$ . Thus when  $[B/B_0]^{1/3}$  is unity the current propagates with the full initial buoyancy, and the two values of  $K$  are equal. However, if  $K_M < K_B$ , as in fact observed, then the ratio  $[B/B_0] = [K_M/K_B]^3$  and a measure of the buoyancy loss to the driving part of the current, the head, can be estimated. Note also that the Beghin *et al.* (1981) equation has been modified in two ways. Firstly, their equation (3) has been used to translate from their growth rate  $\alpha$  to the present measured  $\alpha_0$ , i.e.  $\alpha = [2S_1/S_2 k^{1/2}] \alpha_0$ , while their equation (4), for  $L$  versus  $x$ , has been used to correct from their centre of mass coordinate system to the present system that uses the nose location as the most conveniently measurable quantity, i.e. a difference of  $L/2$ , where  $L$  is the length of the head region. On plotting (3.4) it was found that the dependence on  $k$  was weak and that the main effects were due to

the  $\sin \theta / \alpha_0^2$  combination, so a value of  $k = 0.25$  has been used in what follows, as in Maxworthy & Nokes (2007).

#### 4. Results

In what follows the values  $\theta = 10.6^\circ$  and  $\theta = 5.9^\circ$  were considered for each value of  $L_0$  and  $H_0$  in table 1 for a total of 60 experiments. To make for a more compact presentation only a few cases will be considered in enough detail to make the different flow states clear and to indicate the important dynamical processes at work. Other cases will be treated briefly by giving only essential details and by referring to the details of earlier cases as needed. The experimental results are summarized in table 2(a, b).

##### 4.1. $\theta = 10.6^\circ$ ; $L_0 = 20.1$ cm; $H_0 = 9.7$ cm

This case is a direct extension of the only lock geometry considered in Maxworthy & Nokes (2007). In figure 2 a series of photographs shows the evolution of the current beyond that seen in Maxworthy & Nokes (2007). After the gate was opened a small, well-defined head formed quickly on the outflow followed by the rest of the lock charge (figure 2a). A feeding current joined the two. As time proceeded the following volume collapsed to produce a thin, down-flowing layer of heavy fluid that persisted until about  $x = 100$  cm (figure 2c). Thereafter the head lost its relatively compact shape, split and left behind a great deal of buoyant fluid. In the final stage (figures 2e and 3e) the ‘active’ head was still quite short, approximately 35–40 cm long, followed by a diffuse cloud of negatively buoyant fluid. The term ‘active’ is used here, and elsewhere, to indicate the region between the nose of the current and a clockwise-rotating vortex that separated the head from the following fluid. Here clockwise is to indicate the sense of rotation in the views of figure 2. The rotor can be seen quite clearly at early times at the rear of the head in figure 2(a–c).

One of the more interesting discussions that can be extracted from photographs like those of figure 2 is an explanation of the evolutionary process of the current from its release to the final state reached here. To help this discussion somewhat idealized sketches like those of figure 3 are very useful.

The main observations are outlined in the caption to figure 3. However, several points should be emphasized and enlarged upon. Upon opening the lock gate a two-layer outflow/inflow was formed (figure 3a). Based on intuition one might expect this state to continue indefinitely. However, the intense shear over the inflow/outflow caused both to evolve into antisymmetric, compact head regions in this Boussinesq limiting flow. The inflow head was destroyed by interaction with the end wall, where it plunged to the bottom of the lock and partially mixed with the heavy fluid residing there. In the meantime the outflow head moved down slope both entraining ambient fluid and being fed by the relatively narrow following layer, as in Maxworthy & Nokes (2007). The head maintained its integrity due to the influence of this following inflow at the rear of the head. Further down the slope the head outran the inflow and immediately began to break apart (figure 3d). At each stage thereafter the ‘active head’ continued to grow by the entrainment of ambient fluid and, at the same time, lose buoyancy through the periodic shedding of turbulent vortices into a wake as the Kelvin–Helmholtz instability over the head grew to a very large amplitude and reached the bottom of the channel.

In figures 4–6 are shown some of the diagnostic plots that quantify the picture suggested by the flow visualizations. Figure 4 is the raw data plot of  $x$  versus  $t$  showing the initial acceleration and subsequent deceleration. These are shown more clearly in

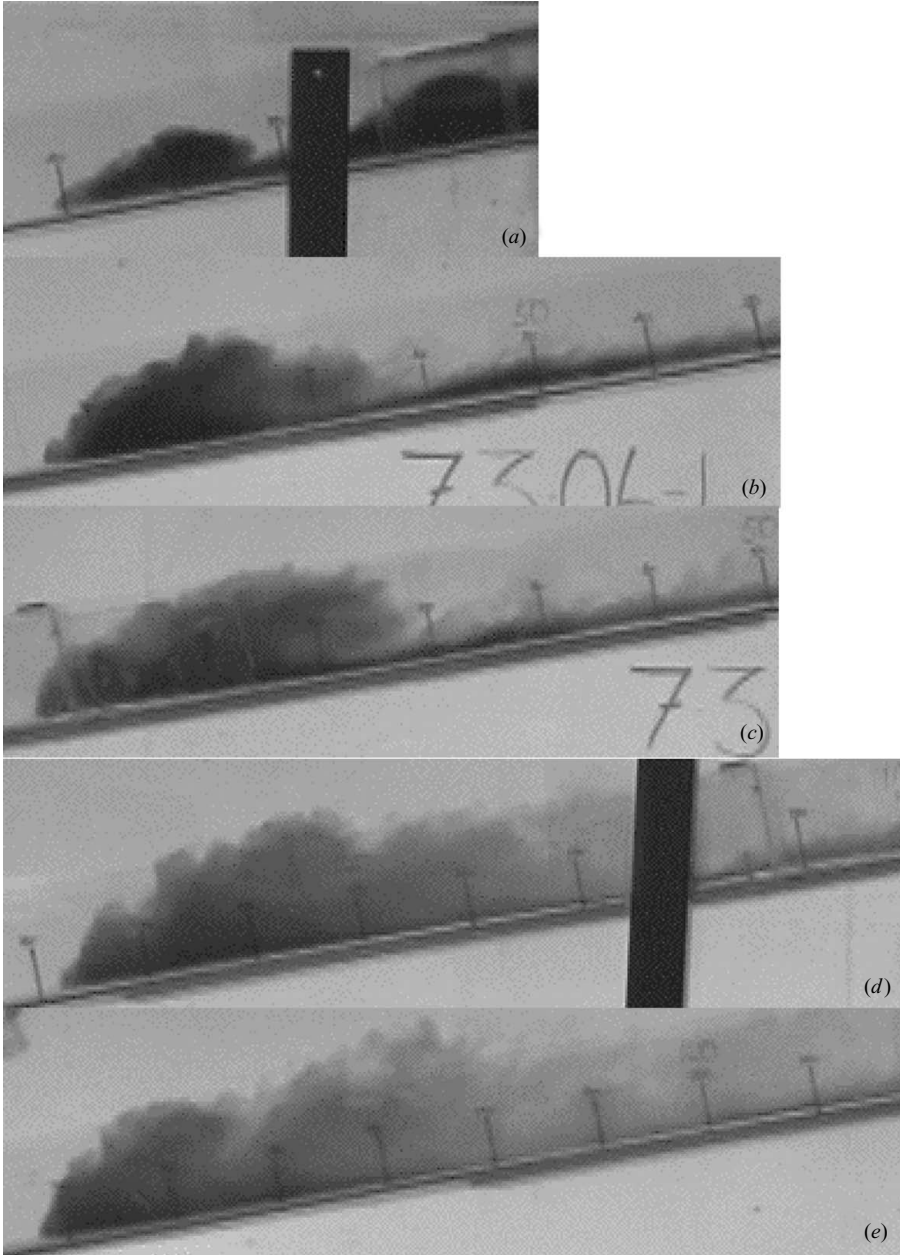


FIGURE 2. Experiment 7/3/06-1. An evolving GC on a  $10.6^\circ$  slope, from a 20.1 cm long, 9.7 cm high lock;  $g'_0 = 12.65 \text{ cm s}^{-2}$ ;  $B_0 = 2467 \text{ cm}^3 \text{ s}^{-2}$ . In (a)  $x = 30 \text{ cm}$ . The head is well formed and is fed by a feeding current from a large following volume. Also, note the head formed on the upper layer moving back into the lock. In (b)  $x = 85 \text{ cm}$ . The head is still well developed with a weakened or, perhaps, zero-flux feeding current. In (c)  $x = 105 \text{ cm}$ . The head is beginning to break up, as the feeding current has zero or close to zero flux into the head. In (d)  $x = 168 \text{ cm}$ . Feeding-current flux is zero. The head is mixing strongly from the rear and is spreading rapidly. In (e)  $x = 212 \text{ cm}$ . Final stage: substantial buoyancy has been shed into the following, low-velocity flow. The vertical marks are 10 cm apart. Unfortunately due to the limited resolution of the photographs taken from video tape their numerical  $x$  values are indistinct. In order to compensate the  $x$  positions of the nose of the head are given in the caption for each image, while the vertical lines are 10 cm apart.



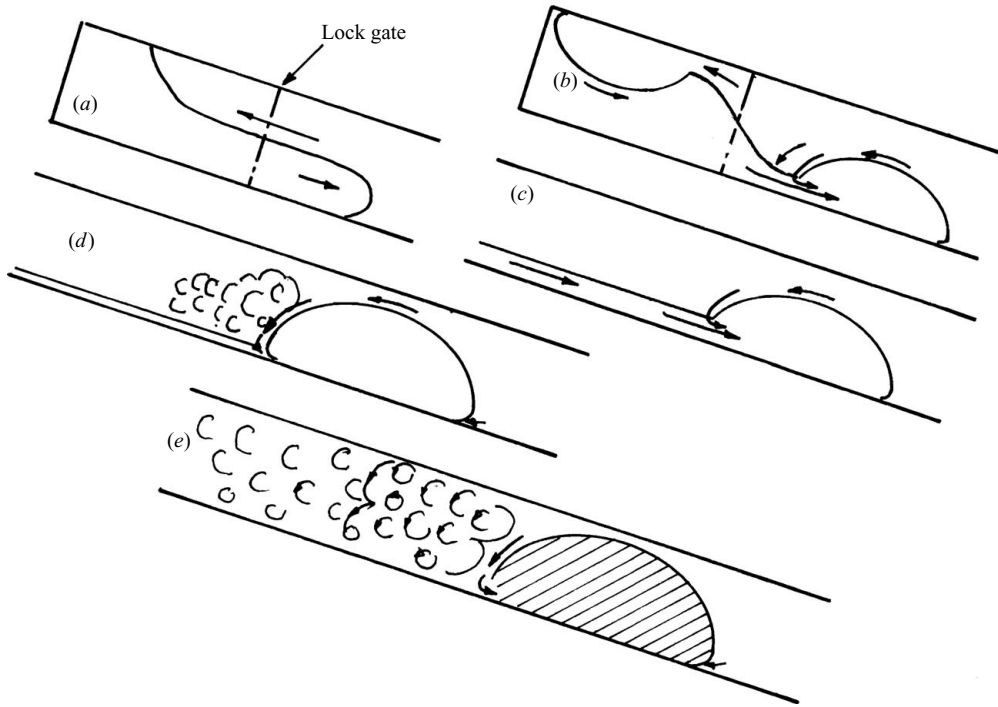


FIGURE 3. Sketches of the evolution of the GC. (a) Upon the rapid withdrawal of the lock gate a two-layer outflow/inflow was formed. The layers were of more-or-less equal height. (b) Head regions formed rapidly from the instability of both the inflow and the outflow (see figure 2a). Especially critical is the distortion of the following outflow layer to less than half of its original thickness by flow over the outflow head. (c) Initially, as in Maxworthy & Nokes (2007), buoyancy was fed into the head by inflow from the following layer. (d) At this stage the inflow had stopped, and the head immediately began to shed buoyancy to a wake-like structure. However, the head was still entraining ambient fluid over its surface and into its rear. (e) The final stage in which more ambient fluid was entrained while, periodically, buoyancy was shed from the rear of the head. The shaded area is what is called the ‘active head’ in the text.

figure 5 where the velocity,  $U$ , is shown as a function of  $x$  for two cases. This result was plotted from the differentiation of a sixth-order fit to the  $x$  versus  $t$  data and shows, in one case, that the maximum velocity  $U_{max}$  of  $8.9 \text{ cm s}^{-1}$  ( $Fr_{max} = U_{max}/(H_0 g'_0)^{1/2} = 0.84$ ) was achieved at  $x = 100 \text{ cm}$ . Due to the nature of the curve fitting over a restricted range of  $x$  the velocities near the end points are contaminated by the lack of data before  $x = 0$  and beyond  $x = 200 \text{ cm}$  and, in particular, do not show a possible  $x^{-1/2}$  behaviour at larger  $x$ , and their values also do not start from zero at  $x = 0$ . Six experiments were run for the same geometric conditions but different values of  $g'$ . The average value  $Fr_{max}$  was found to be  $0.83 \pm 0.01$ ; however, as shown in figure 5 the  $U$  versus  $t$  plots had two very different basic shapes. Of the six experiments three had one maximum; two had two maxima; and the sixth was somewhere between the two. This observation is certainly a partial explanation for the substantial scatter found in the Maxworthy & Nokes (2007) experiments and is most certainly the result of different turbulent evolutions of the heads each case.

In order to examine the long-term behaviour the data was replotted as  $(x + x_0)^{3/2}$  versus  $t$ , with  $x_0$  found as discussed before. This form was used with the

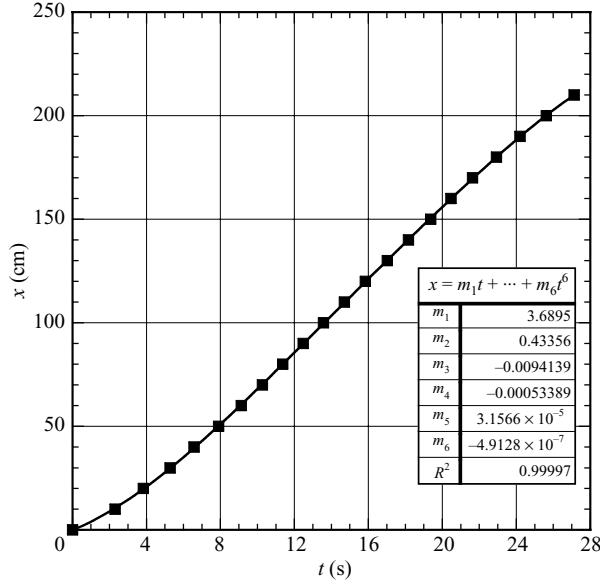


FIGURE 4. Experiment 6/3/06-3:  $x$  versus  $t$  for  $A_0^{1/2} = 13.9$  cm;  $g'_0 = 11.58$  cm s $^{-2}$ ;  $B_0 = 2246$  cm $^3$  s $^{-2}$ ;  $L_0 = 20.0$  cm;  $H_0 = 9.7$  cm.

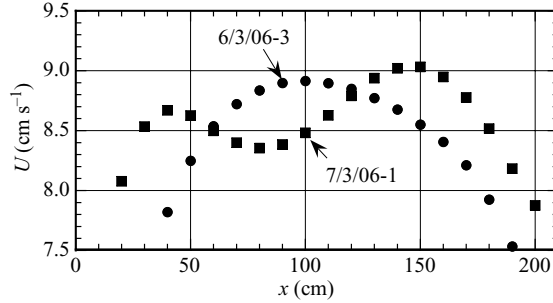


FIGURE 5. Experiments 6/3/06-3 and 7/3/06-1, showing differences in velocity history for similar initial parameter values ( $g'_0$  is of the order of 12 cm s $^{-2}$ ). 6/3/06-3:  $Fr_{max} = 0.84$ . 7/3/06-1: first  $Fr_{max} = 0.78$ ; second  $Fr_{max} = 0.81$ .

background knowledge that the Beghin *et al.* (1981) theory gives a decay of the form  $x + x_0 = \text{const } t^{2/3}$ , for constant buoyancy, but as will be seen this seems to be an oversimplification. Figure 6 is the result of such a plot for experiment 6/3/06-3.

Based on the curve fit shown one can calculate that the decay region is given by

$$(x + x_0) = 2.58 B_0^{1/3} (t + t_0)^{2/3}$$

if one assumes the buoyancy does not vary. The average value of the constant over the six experiments was  $2.66 \pm 0.06$ . From this comes the first clue as to the processes involved, since if one uses the Beghin *et al.* (1981) theory, i.e. (3.3), to calculate the value for this constant with the full initial value of  $B_0$  one finds magnitudes that are considerably larger than this, suggesting that the full buoyancy is not acting on the current at this late stage. This point is raised here to indicate that it will be a continuing observation and a major component of the discussion section (§5)

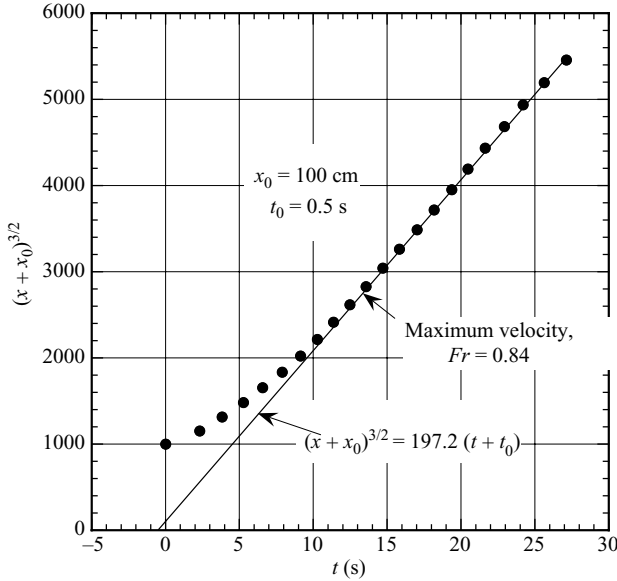


FIGURE 6. Experiment 6/3/06-3:  $(x + x_0)^{3/2}$  versus  $t$  for  $A_0^{1/2} = 13.9$  cm;  $g'_0 = 11.58$  cm s $^{-2}$ ;  $B_0 = 2246$  cm $^3$  s $^{-2}$ . The line shown is the best fit straight line to the final decay and gives a value for the multiplicative constant (197.2 in this case) in the fitting equation. In this case the maximum velocity ( $Fr_{max} = 0.84$ ) occurs at about  $t = 13.5$  s and  $x = 100$  cm.

together with a commentary on the connection between the flow visualizations and the quantitative data.

#### 4.2. $\theta = 5.9^\circ$ ; $L_0 = 20.1$ cm; $H_0 = 9.7$ cm

Since the equivalents to figures 2–6 are similar for this case only the measured average parameter values will be presented. There was still an extensive acceleration region in three experiments with a maximum velocity reached at  $x = 125 \pm 15$  cm with the maximum  $Fr = 0.75 \pm 0.03$ . The final decaying phase of the motion gave an average value of  $K_M$ , over the three experiments, of  $2.94 \pm 0.10$ .

#### 4.3. $\theta = 10.6^\circ$ ; $L_0 = 10.2$ cm; $H_0 = 10.1$ cm

This case is the next logical one to consider after the one discussed in §4.1. The lock was essentially half as long and also approximately 10 cm high, with half the initial volume/unit width. Although this case has many similarities with the previous ones there are subtle differences that need to be explored. Figure 7 is the first evidence of these differences.

The initial motion has, as might be expected, a far smaller feeding current and trailing volume. This results in a shorter acceleration period and a maximum velocity reached much sooner than previous examples. Figure 8 quantifies this effect with a maximum velocity reached at approximately half the distance found with the 20 cm long lock. A  $t^{-1/3}$ -like velocity decay appears to start almost immediately after the maximum velocity peak, but the detailed analysis in §5, and below, shows that this is not correct. As before end points should be ignored in these data from the curve fit to the  $x$  versus  $t$  data. Plots of  $x$  versus  $t$  and  $(x + x_0)^{3/2}$  versus  $t$  are similar in form to those found before and need not be shown. Averaging four experiments gives  $Fr_{max} = 0.78 \pm 0.02$ , occurring on average at  $x = 56 \pm 5$  cm while  $K_m = 2.89 \pm 0.09$  with  $x_0 = 110 \pm 10$  cm.

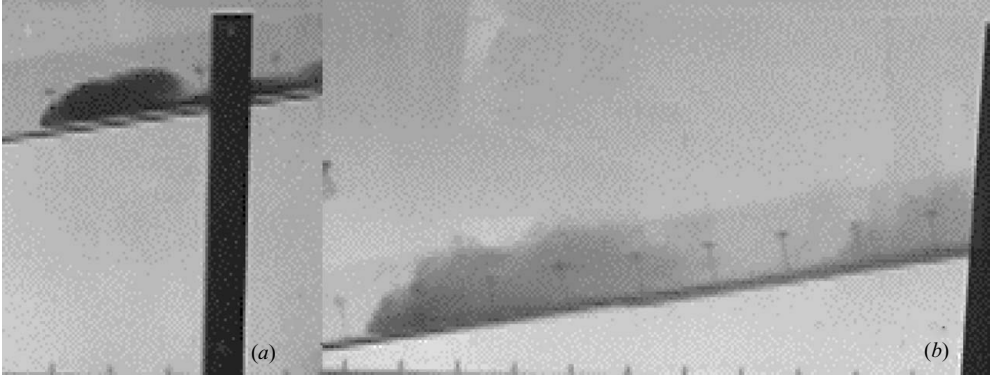


FIGURE 7. Experiment 17/2/06-1. Two photographs of the current, for the conditions  $\theta = 10.6^\circ$ ,  $L_0 = 10.2$  cm,  $H_0 = 10.1$  cm,  $g'_0 = 15.50$  cm s $^{-2}$ ,  $B_0 = 1597$  cm $^3$  s $^{-2}$  (a) at the beginning of the motion and (b) at the end. In (a) the head is well formed, but the following volume and the feeding current are small, leading to a more rapid attainment of the maximum velocity. In (b) the leading head is well formed but has left behind a large volume of negatively buoyant fluid. The thick black vertical line in (a) is one of the side-wall support posts.

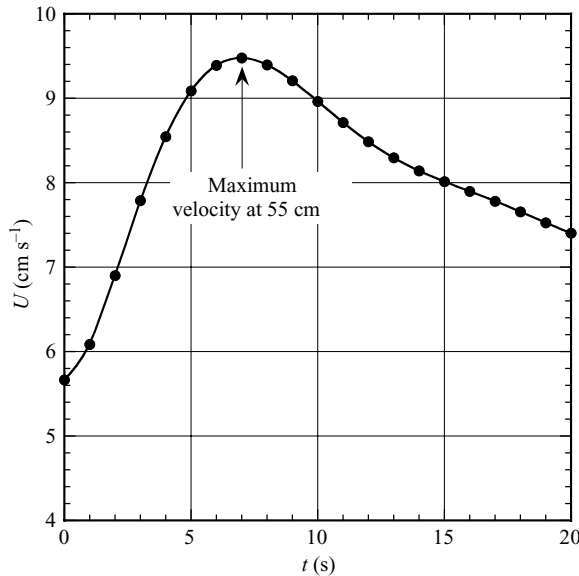


FIGURE 8. Experiment 17/2/06-1:  $U$  versus  $t$  for  $\theta = 10.6^\circ$ ;  $L_0 = 10.2$  cm;  $H_0 = 10.1$  cm;  $g'_0 = 15.50$  cm s $^{-2}$ ;  $B_0 = 1597$  cm $^3$  s $^{-2}$ . The maximum velocity is reached only a short distance down the channel with  $Fr_{max} = 0.75$ .

A much later experiment (18/9/07) in this sequence was undertaken using the dye/luminosity technique of § 2 in order to unambiguously identify the buoyancy loss during the later stages of head motion. For this case  $g'_0 = 53.3$  cm s $^{-2}$  and  $B_0 = 5490$  cm $^3$  s $^{-2}$ , and the relevant experimental result for the decay was  $(x + x_0) = 2.70B_0^{1/3}(t + t_0)^{2/3}$  as discussed in detail in § 5, figure 16. Figure 9(a-c) shows the result of the measurements of average dimensionless density difference between the head and its surroundings, area and buoyancy  $B/B_0$  versus  $x$ . One must assume that during the increasing part of the  $B/B_0$  history dense fluid was being added

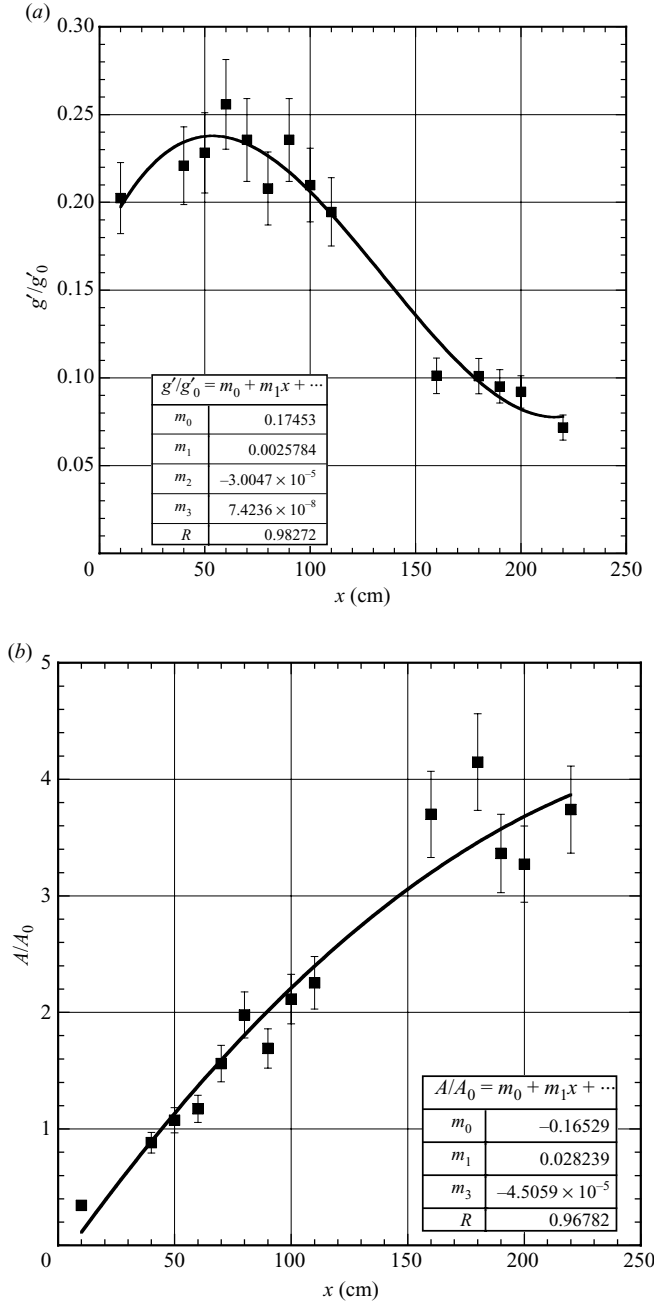


FIGURE 9. For caption see next page.

to the head from the following current and that during the decreasing part it was being lost to a wake. A study of the video record suggests that the transition between the two was quite abrupt, since the head form changed quite dramatically when the stabilizing influence of the following flow was lost. Of course the interesting result here is that it appears the  $t^{2/3}$  dependence is quite good even though the buoyancy is not constant. This apparent contradiction and related matters will be discussed in § 5.

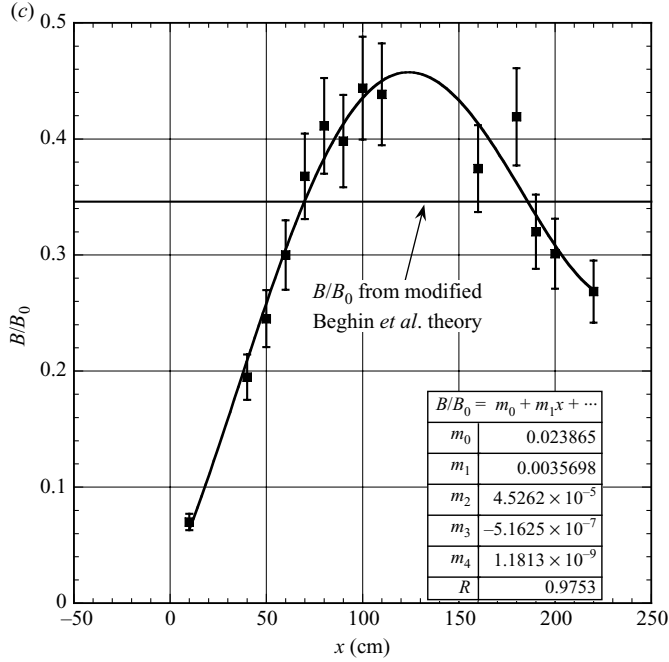


FIGURE 9. (a–c). Test 18//9/07. Dimensionless average head density difference, area and total buoyancy versus  $x$ , for the initial conditions  $g'_0 = 53.3 \text{ cm s}^{-2}$ ,  $B_0 = 5330 \text{ cm}^3 \text{ s}^{-2}$ ,  $L_0 = 10 \text{ cm}$  and  $H_0 = 10 \text{ cm}$ . The gaps in the data are due to the shielding of the head by the sidebar supports of the tank.

#### 4.4. $\theta = 5.9^\circ$ ; $L_0 = 10.2 \text{ cm}$ ; $H = 10.1 \text{ cm}$

Again this series of four experiments have characteristics similar to those that have gone before except for a change in trend shown in figure 10. The approach to the  $t^{2/3}$  decay is from below in all experiments in contra-distinction to the previous cases in which it was from above. This effect seems to be typical of experiments with a ‘low’ driving force, i.e. small angle or smaller lock dimensions. An extreme example is shown in §5, figure 17. As before there was a substantial loss of negatively buoyant fluid before the head reached the end of the channel. The averaged resulting parameters for the series of four experiments are  $Fr_{max} = 0.71 \pm 0.04$  at  $x = 59 \pm 6 \text{ cm}$ , while the averaged  $K_M = 2.78 \pm 0.04$ .

#### 4.5. $\theta = 10.6^\circ$ ; $L_0 = 5.5 \text{ cm}$ ; $H_0 = 9.7 \text{ cm}$

The case has, yet again, half the length and volume of the preceding case. Photographs of the initial, intermediate and final head shapes are shown in figure 11.

The  $x$  versus  $t$  representation (figure 12) shows a very smooth transition from a short acceleration period to a nominal  $t^{2/3}$  behaviour (figure 13) with a sizeable intermediate region. Although the latter transition is quite difficult to determine exactly the agreement with the  $2/3$  law is, at first sight, good but slightly smaller exponents gave a better statistical fit. Over six experiments, for different values of  $g'_0$ , the average  $Fr_{max} = 0.70 \pm 0.05$  at  $x = 41 \pm 2 \text{ cm}$ , while  $K_M = 2.94 \pm 0.07$ .

This geometry was chosen as a second test using the dye/luminosity technique with  $g'_0 = 51.5 \text{ cm s}^{-2}$  and  $B_0 = 2750 \text{ cm}^3 \text{ s}^{-2}$ . For the decaying phase of the motion

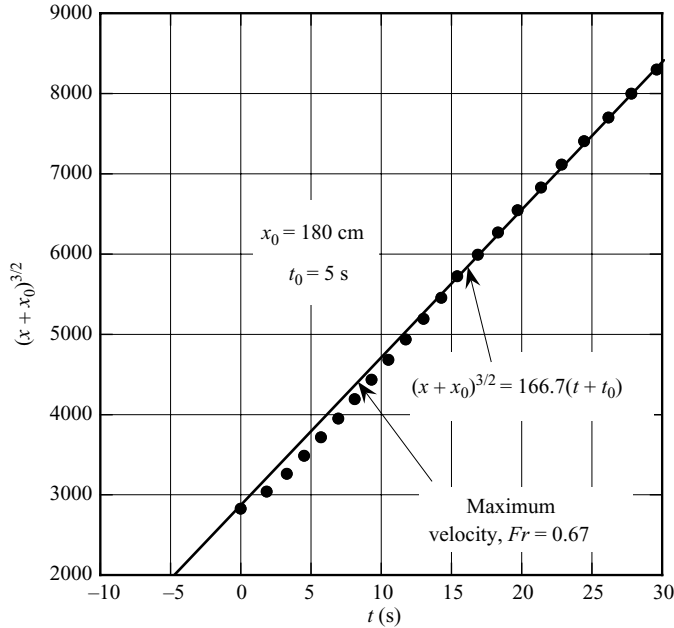


FIGURE 10. Experiment 17/2/06-5:  $(x + x_0)^{3/2}$  versus  $t$  for  $\theta = 5.9^\circ$ ;  $t_0 = 10.2$  cm;  $H_0 = 10.1$  cm;  $g'_0 = 15.5$  cm s $^{-2}$ ;  $B_0 = 1597$  cm $^3$  s $^{-2}$ . In this case, as distinct from those that have gone before, the approach to the straight line representing the expected decay is from below.

$(x + x_0) = 2.85B_0^{1/3}(t + t_0)^{2/3}$ , while the plots of the dimensionless average density difference, area and total buoyancy as functions of  $x$  are shown in figure 14(a-c).

Here the buoyancy loss is larger than in the previous case, but the modified Beghin *et al.* (1981) theory appears to describe the loss reasonably well.

$$4.6. \theta = 5.9^\circ; L_0 = 5.5 \text{ cm}; H_0 = 9.7 \text{ cm}$$

The results for this geometry are similar to those immediately above. A well-formed head appears immediately upon release of the lock charge, accelerates quickly to its maximum velocity and then mixes violently as it propagates down the channel, leaving a trail of dense fluid that is almost uniform (figure 15). The final head is, again difficult to distinguish from the still photographs, but the videos show that the following vortex that closes the head is about 25 cm long and 7.2 cm high, i.e.  $k = H/L = 0.26$ . From three experiments  $Fr_{max} = 0.67 \pm 0.05$  at  $x = 40 \pm 1$  cm, while  $K_M = 2.61 \pm 0.01$ .

#### 4.7. A brief presentation of experiments with nominally 5 cm and 2.5 cm high locks.

The results for these locks are superficially similar to those described above when plotting  $x$  versus  $t$  or when viewing the raw photographs. However, differences become apparent when plotting  $(x + x_0)^{3/2}$  versus  $t$ . The tendency to a nominal straight line fit is somewhat different from case to case. This suggests that subtle differences in buoyancy loss and gain are present that are not obvious from simply studying the videos of the head evolution. In general the values of  $K_M$  are smaller than for the deeper locks, while the initial motion, for all of the  $5.9^\circ$  cases, seems to follow an initial law that is close to one that varies as  $t^{2/3}$  before transitioning to the final  $t^{2/3}$  relationship (see § 5, figure 17). It is possible that for these weaker currents the head

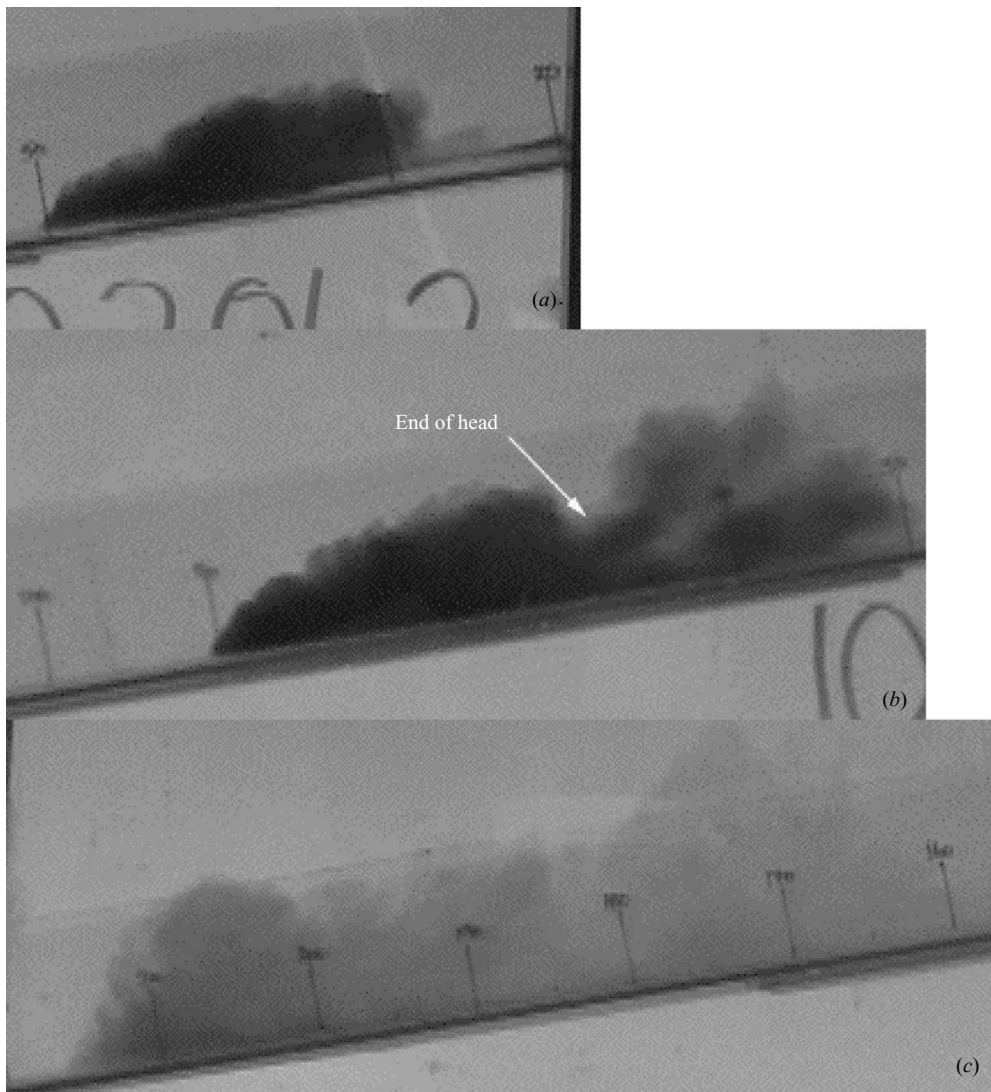


FIGURE 11. Experiment 10/2/06-1.  $L_0 = 5.5$  cm,  $H_0 = 9.7$  cm,  $g'_0 = 29.23$  cm s $^{-2}$ ;  $B_0 = 1559$  cm $^3$  s $^{-2}$ . Showing that just after reaching maximum velocity in (a) at  $x = 50$  cm the feeding current has no input into the head. In (b)  $x = 90.5$  cm; here a substantial volume of heavy fluid has been rejected rearwards, leaving the head with lowered buoyancy. In (c)  $x = 215$  cm. In the final stages the head is very diffused with no clear demarcation of its rear end. From the video it is possible to pick out the location at which the trailing vortex ends near the mark 180 cm, i.e. the third vertical marking from the right. These lengths are actually 55, 95.5, 220 and 185 cm from the lock gate, since the shortening of the lock changed the zero position, while the markings themselves were not changed.

Reynolds numbers ( $UH/\nu$ , where  $U$  is the head velocity,  $H$  its maximum height and  $\nu$  the fluid kinematic viscosity) were low enough for viscous effects to be more important than in the deeper lock cases. Values in the range 1000–2000 were estimated for these cases. In previous work values in this range were thought to give results independent of viscous effects, but this may not be true here. Values of  $K_M$ ,  $x_0/A_0^{1/2}$  and  $t_0/(A_0^{1/4}/g_0^{1/2})$  for these cases are given in table 2(b) in § 5.



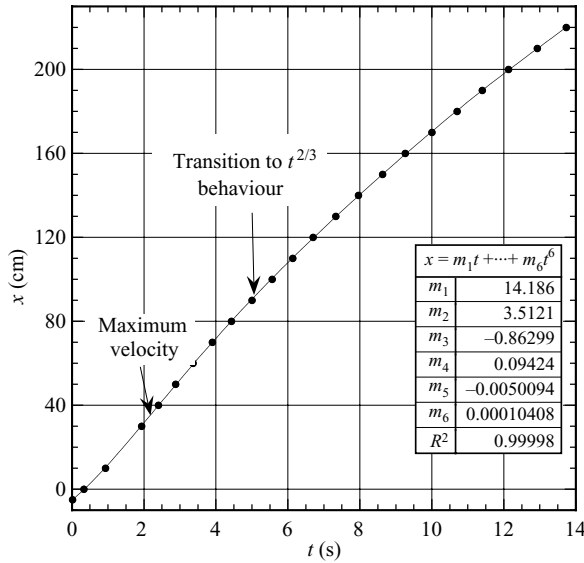


FIGURE 12. Experiment 10/2/06-4:  $x$  versus  $t$  for  $\theta = 10.6^\circ$ ,  $L_0 = 5.5$  cm,  $H_0 = 9.7$  cm,  $g'_0 = 99.57$  cm s<sup>-2</sup> and  $B_0 = 5203$  cm<sup>3</sup> s<sup>-2</sup>, showing a very rapid rise to the maximum velocity and a slow transition to a nominal  $t^{2/3}$  behaviour, due to the substantial vortex/buoyancy shedding shown in figure 11(b).

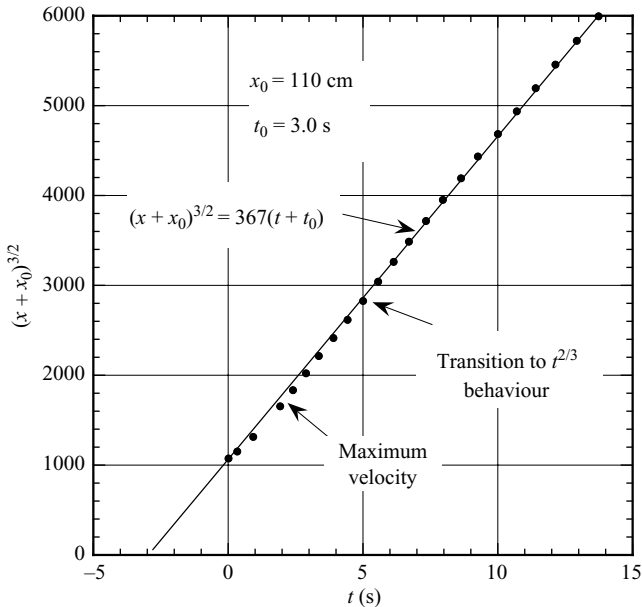


FIGURE 13. Experiment 10/2/06-4. Same conditions as figure 12. The region between the point of maximum velocity and the transition to  $t^{2/3}$  behaviour is the time taken to shed a major portion of the initial buoyancy, as shown in figure 11(b).

### 5. Discussion and conclusions

The main discussion concerns the observation that much of the initial charge either never enters or is eventually lost from the leading head region so that it would seem reasonable to expect that the final decay stage would be described by a law that

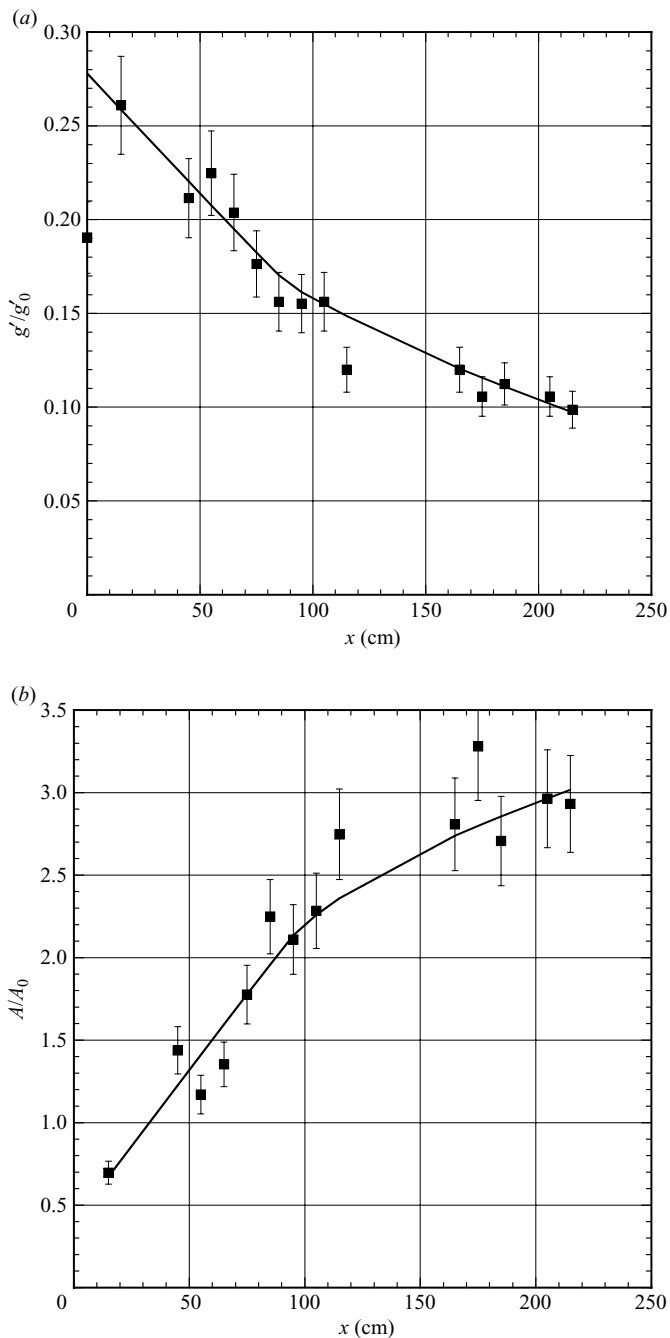


FIGURE 14. For caption see facing page.

reflects this fact. Using the theory of Beghin *et al.* (1981) one can quantify this effect to some degree. As discussed in §3.1, theory can be cast in a form that allows direct comparison with the experimental measurements. Thus the decay law can be written as in the results section as

$$(x + x_0) = K_B B_0^{1/3} (t + t_0)^{2/3},$$

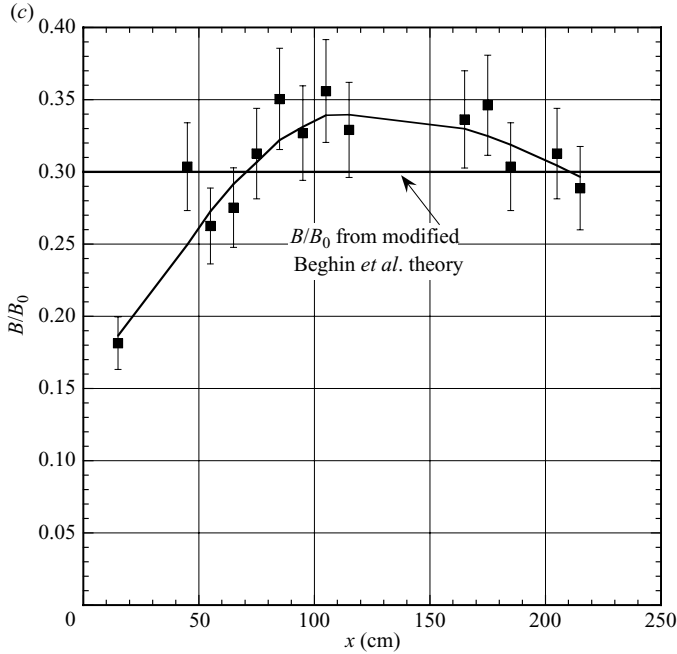


FIGURE 14. (a–c). Experiment 25/1/08:  $L_0 = 5.5$  cm,  $H_0 = 9.7$  cm. Dimensionless average density difference, area and total buoyancy versus  $x$ . Initial conditions are  $g'_0 = 51.5$  cm s $^{-2}$  and  $B_0 = 2750$  cm $^3$  s $^{-2}$ .

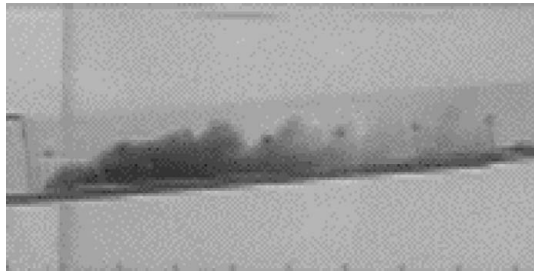


FIGURE 15. Experiment 15/2/06-3:  $\theta = 5.9^\circ$ ;  $L_0 = 5.5$  cm;  $H_0 = 9.7$  cm;  $g'_0 = 25.80$  cm s $^{-2}$ ;  $B_0 = 1348$  cm $^3$  s $^{-2}$ . Showing that the initial head has mixed extensively when its nose is 115 cm from the lock. The buoyancy is distributed over approximately 60 cm or  $11L_0$ . The head is closed about 25 cm behind the nose and  $k \approx 0.26$ .

where  $K_B$  is the equivalent of the experimentally measured quantity  $K_M$ . Then from the Beghin *et al.* (1981) theory one can estimate the effective buoyancy ( $B$ ) acting on the GC head as

$$[B/B_0] = [K_M/K_B]^3.$$

On plotting (3.4) it was found that in the range of interest the dependence of  $K_B$  on  $k$  was weak and that the main effects were due to the  $\sin\theta/\alpha_0^2$  combination, so a value of  $k = 0.25$  has been used here, as in Maxworthy & Nokes (2007). Then based on the values of the coefficients  $K_M$  reported in the table 2(a) can be constructed for the cases with  $H_0$  nominally equal to 10 cm.

Angle	$L_0$ (cm)	$K_M$	$\alpha_0$	$K_B$	$K_M/K_B$	$B/B_0$
$\theta = 10.6^\circ$	20.1	$2.66 \pm 0.04$	$0.037 \pm 0.005$	$3.69 \pm 0.4$	$0.72 \pm 0.1$	$0.37^{+0.18}_{-0.13}$
	10.1	$2.89 \pm 0.09$	$0.033 \pm 0.005$	$4.05 \pm 0.4$	$0.71 \pm 0.11$	$0.36^{+0.19}_{-0.14}$
	5.5	$2.94 \pm 0.07$	$0.025 \pm 0.008$	$4.66 \pm 1.1$	$0.63 \pm 0.22$	$0.25^{+0.36}_{-0.18}$
$\theta = 5.9^\circ$	20.1	$2.84 \pm 0.10$	$0.031 \pm 0.005$	$3.44 \pm 0.4$	$0.82 \pm 0.14$	$0.55^{+0.33}_{-0.23}$
	10.1	$2.70 \pm 0.04$	$0.029 \pm 0.03$	$3.60 \pm 0.2$	$0.75 \pm 0.02$	$0.42^{+0.04}_{-0.03}$
	5.5	$2.61 \pm 0.01$	$0.025 \pm 0.006$	$3.84 \pm 1.0$	$0.68 \pm 0.24$	$0.31^{+0.47}_{-0.22}$

TABLE 2a. Table showing the estimated effective buoyancy ratio,  $B/B_0$ , during the decaying phase for all the experiments of table 1 for which  $H_0$  is nominally 10 cm.

Angle	$L_0$ (cm)	$H_0$ (cm)	$L_0/H_0$	$K_M$	$x_0/A_0^{1/2}$	$t_0/(A_0^{1/4}/g_0^{1/2})$	$Fr_{max}$
$\theta = 10.6^\circ$	20.1	9.7	2.07	$2.66 \pm 0.04$	$7.9 \pm 0.7$	$1.59 \pm 1.42$	$0.83 \pm 0.01$
	10.0	5.0	2.00	$2.77 \pm 0.05$	$11.2 \pm 1.1$	$3.81 \pm 2.3$	$0.77 \pm 0.03$
	5.5	2.5	2.00	$2.62 \pm 0.14$	$16.2 \pm 2.7$	$28.9 \pm 8.5$	$0.79 \pm 0.05$
	10.1	10.0	1.01	$2.89 \pm 0.09$	$10.9 \pm 1.0$	$4.79 \pm 1.3$	$0.78 \pm 0.02$
	5.0	5.0	1.00	$2.53 \pm 0.10$	$13.3 \pm 1.9$	$16.7 \pm 3.5$	$0.75 \pm 0.04$
	5.5	9.65	0.57	$2.94 \pm 0.07$	$12.5 \pm 1.4$	$9.30 \pm 5.1$	$0.70 \pm 0.05$
$\theta = 5.9^\circ$	20.1	9.7	2.07	$2.84 \pm 0.10$	$14.6 \pm 1.4$	$11.2 \pm 1.2$	$0.75 \pm 0.03$
	10.0	5.0	2.00	$2.47 \pm 0.03$	$29.0 \pm 1.4$	$28.4 \pm 20.5$	$0.72 \pm 0.02$
	5.5	2.5	2.00	$2.45 \pm 0.15$	$16.1 \pm 2.7$	$44.1 \pm 15.8$	$0.75 \pm 0.09$
	10.1	10.0	1.01	$2.70 \pm 0.04$	$17.8 \pm 2.0$	$17.1 \pm 1.5$	$0.71 \pm 0.04$
	5.0	5.0	1.00	$2.36 \pm 0.12$	$12.7 \pm 2.0$	$46.1 \pm 14.2$	$0.66 \pm 0.02$
	5.5	9.65	0.57	$2.61 \pm 0.01$	$25.7 \pm 2.8$	$10.5 \pm 2.8$	$0.67 \pm 0.05$

TABLE 2b. The dimensionless dependent variables  $K_M$ ,  $x_0/A_0^{1/2}$ ,  $t_0/(A_0^{1/4}/g_0^{1/2})$  and  $Fr_{max}$  as they depend on  $\theta$  and  $L_0/H_0$ . Each value is the average of between four and eight experiments. The error estimates are to add and subtract the maximum and minimum values and are not the r.m.s. estimates.

Table 2(b) is a compilation of the interesting dimensionless dependent variables for the whole range of experiments. They are arranged by channel angle and lock aspect ratio,  $L_0/H_0$ , and include  $K_M$ ,  $x_0/A_0^{1/2}$ ,  $t_0/(A_0^{1/4}/g_0^{1/2})$  and  $Fr_{max}$ .

The results shown in table 2(a,b) allow for some interesting conclusions. Starting with table 2(a). The results for  $B/B_0$  are surprisingly consistent, although the error estimates, which represent the maximum and minimum and not root mean square (r.m.s.) values, are very large. Nonetheless, the results point to both an incomplete capture of the initial buoyancy,  $B_0$ , and a sizeable buoyancy loss during the decay phase of the motion, as found by the dye-transmissivity technique and noted below. Even though the values of  $K_M$  tend to increase with decreasing  $L_0$  the resulting values of  $B/B_0$  are reduced, as  $L_0$  is reduced, and increased for the smaller value of  $\theta$ .

The results of the dye/luminescence experiments can be used to support these results and the consequences that follow from them. For the first case, 18/9/08, with a 10 cm  $\times$  10 cm lock and  $\theta = 10.6^\circ$  the value of  $K_M = 2.70$ , as presented earlier. Based on the measurements of the head geometry as it propagates, i.e.  $\alpha_0$  and  $x_0$ , and using (3.3) the value of  $K_B$  that results is 3.95. Thus  $K_M/K_B = 0.683$  so that  $B = 1765$  and  $B/B_0 = 0.321 \text{ cm}^3 \text{ s}^{-2}$ . This latter value is plotted in figure 7(b), where it is seen to fall at approximately the average value of  $B$  during the decay phase.

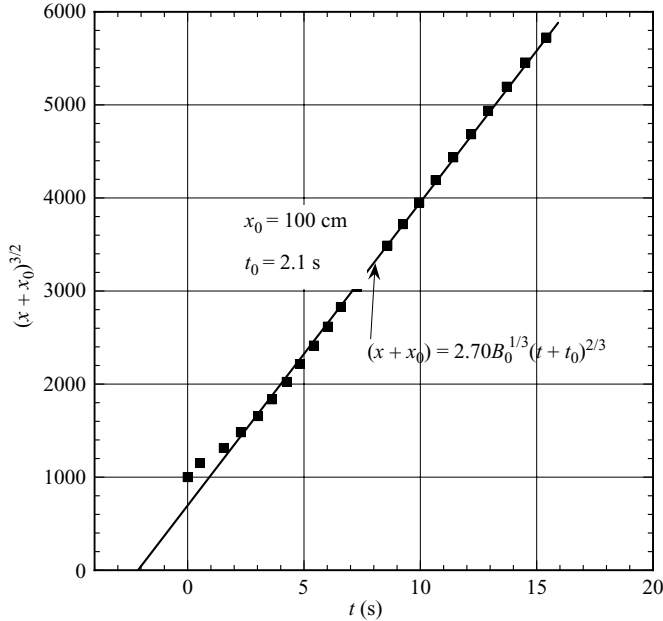


FIGURE 16. Experiment 18/9/07. This is the case described in detail in figure 9:  $L_0 = 10$  cm,  $H_0 = 10$  cm;  $(x + x_0)^{3/2}$  versus  $(t + t_0)$  with  $x_0 = 100$  cm and  $t_0 = 2.1$  s, showing that the quoted equation describes the evolution from somewhat before the decay phase as well as the decay phase itself, which starts at around 8 s, i.e. at the location of the arrowhead.

What is even more striking is that  $K_M = 2.70$  actually describes the evolution over a much larger range of time or distance than even the decay phase, as shown in figure 16.

Thus it appears that the averaged equation can describe the consequences of both the late part of the increase and all of the decrease in buoyancy shown in figure 7(b), to a very good degree of accuracy. If one were not aware of the details of the buoyancy history one would be tempted to conclude, based on figures like figure 16, that the decay started much sooner than it actually did, a rather surprising finding, and that the  $t^{2/3}$  behaviour is a good fit to the data under many circumstances.

Carrying out this same type of analysis on experiment 25/1/08 with a lock that was 10 cm high and 5 cm long gave  $K_M = 2.85$ ,  $K_B = 4.25$ ,  $B/B_0 = 0.30$  and  $B = 825 \text{ cm}^3 \text{ s}^{-2}$ . This result is plotted in figure 14(c), where again it lies within the variation of  $B/B_0$  found directly. A plot like that presented in figure 16 again shows that the averaged equation describes both part of the increasing, to a good approximation, and all of the decreasing part of the buoyancy variation.

Also, note that the values for  $\alpha_0$  for the longer lock are slightly smaller than those given in Maxworthy & Nokes (2007) and Beghin *et al.* (1981). This is the result of measuring them only over the decaying part of their  $U$  versus  $t$  history and does not include the period during which buoyancy and mass were being added to the head region.

The results shown in table 2(b) are less readily explained without making radical assumptions. Firstly, while the trends in  $Fr_{max}$  are consistent with intuition, i.e. the values decrease with decreasing  $\theta$ , there appears to be no reasonable scaling law between them. For example, the power law relationship between  $Fr_{max}$  and the logical choice  $\sin \theta$  does not appear to depend on any plausible exponent, e.g. one half. So

the results just stand as a measured consequence of the experiments. The variations of  $Fr_{max}$  with the dimensions of the lock, at any one of the two slopes, appear to scale with the lock aspect ratio in three out of the four cases in which there is more than one experiment to make such a comparison. The reason for the deviation in the one exceptional case is unclear except to note that it is for the lowest angle and a relatively small lock. This point will be raised again in what follows, where a more complete explanation will be attempted.

Other aspects of the results are more difficult to rationalize. Thus for constant  $L_0/H_0$  and  $\theta$  in table 2(b),  $K_M$ ,  $x_0/A_0^{1/2}$  and  $t_0/(A_0^{1/4}/g_0^{1/2})$  do not appear to be constant as one might expect. Since it was very difficult to measure the very small values of  $\alpha_0$  with great accuracy and then extrapolate over such long distances to zero height, as sketched in figure 1, the errors in  $x_0$  are large. This is then reflected in the error values for the dimensionless quantity  $K_M$  as well. For  $K_M$  one could argue that the values are constant within the error estimates given. Using this approach the average values of  $K_{M(Av)} = 2.73 \pm 0.20$  and  $2.57 \pm 0.21$  for  $\theta = 10.6^\circ$  and  $5.9^\circ$  respectively. Then the dimensionless averaged displacement–time relationship

$$(x + x_0)/A_0^{1/2} = K_{M(Av)} [(t + t_0)/(A_0^{1/4}/g_0^{1/2})]^{2/3}$$

can be used to determine the behaviour over all conditions of buoyancy and geometry, within the limits set by these experiments. Clearly, to obtain the actual motion in physical  $(x-t)$  space one needs to know the values for  $x_0/A_0^{1/2}$  and  $t_0/(A_0^{1/4}/g_0^{1/2})$  for the actual conditions of any proposed experiment. The erratic dependence of these quantities on aspect ratio and slope makes it unclear what the correct scaling might be. For  $x_0/A_0^{1/2}$ , for example, there are only two other independent length scales, namely  $L_0$  and  $H_0$  themselves. Clearly using either of them does not solve the problem, since  $x_0/H_0 = x_0/A_0^{1/2}(L_0/H_0)^{1/2}$ , and with  $L_0/H_0$  assumed constant there is no advantage in using these alternatives. Similarly, using  $t_0/(H_0^{1/2}/g_0^{1/2})$  as the dimensionless version of  $t_0$  results in no advantage over the form chosen. Again one might be tempted to use averaged values except for some large deviations in  $t_0/(A_0^{1/4}/g_0^{1/2})$  in particular. These occur for the smaller locks and the lowest angle and are the result of  $(x + x_0)^{3/2}$  versus  $(t + t_0)$  plots which are quite different from those shown in figures 4, 10, 13 and 16 in which the deviation from the straight line of (3.1) is relatively small over the whole range of any one experiment. A typical case is shown in figure 17, where both  $x$  and  $(x + x_0)^{3/2}$  versus  $t$  are shown. In this case and others like it the maximum velocity was reached very quickly, typically within five or six lock lengths, and the approach to the ultimate  $t^{2/3}$  behaviour was very slow. In fact, there appears to be a region of intermediate  $t^{2/3}$  behaviour after the maximum velocity and before the final decay law. The value of  $K_M$  for this intermediate region is large and would suggest that a large fraction the initial buoyancy was contained in the head. However, a careful study of the video for this period of time was ambiguous on this point, but such a study does show that in many cases transition between the two regimes was accompanied by a large loss of buoyancy in one large eddy, see e.g. figure 11(b). Then the existence of an extensive region before the final decay means that the latter starts later in the sequence, resulting in large values of  $t_0$ . At the same time for these cases  $A_0$  was small so that  $t_0/(A_0^{1/4}/g_0^{1/2})$  is large as noted in table 2(b). As noted previously one might be inclined to speculate that this anomalous behaviour is due to viscous effects, but typical Reynolds numbers are in the range of 1000–2000 over most of the current's evolution. At such values it has been generally felt that viscous forces are not an important effect in the GC force balance, but the present cases might prove to be an exception to this belief.

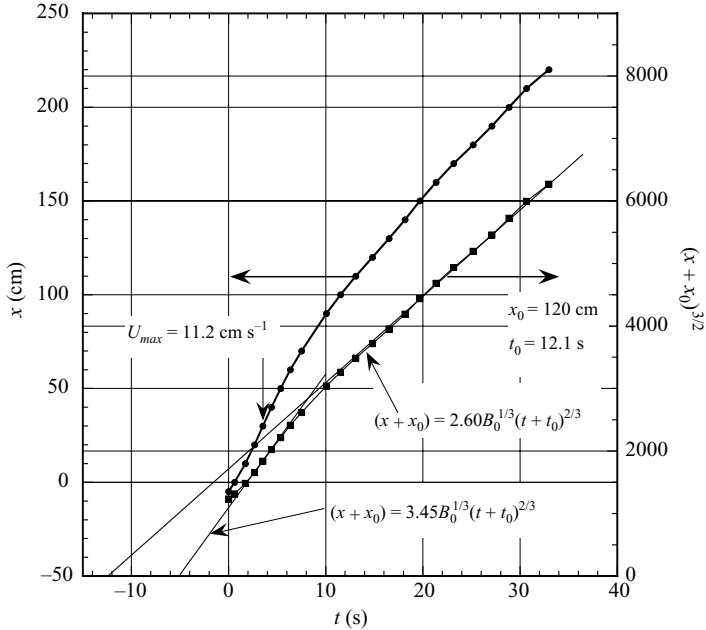


FIGURE 17. Experiment 3/2/06-6 with  $L_0 = 5.5$  cm,  $H_0 = 2.5$  cm,  $\theta = 5.9^\circ$ ,  $g'_0 = 78.7$  cm s $^{-2}$ ,  $B_0 = 1082$  cm $^3$  s $^{-2}$ ;  $x$  and  $(x + x_0)^{3/2}$  versus  $t$ , showing two regions in which the classical decay law seems to apply and the late start of final decay. The quoted value of  $x_0$  applies to both the intermediate and the final decay periods;  $t_0$  applies to the final decay only.

These experiments have confirmed the idea that there is a substantial buoyancy loss from the propagating head. In fact, if the channel had been substantially longer it seems quite likely that all the buoyancy would have eventually been mixed out and that the current would have moved as a long, coherent cloud with distributed buoyancy rather than a denser head with a slower moving tail. This is partially confirmed by the experiments of Laval *et al.* (1988) who showed, in their figure 2, the continuous shedding of buoyancy over a distance of 4 m. It is also characteristic of mixing fronts in long, tilted tubes (see e.g. Seon *et al.* 2007). A similar possibility is suggested by the present experiments, e.g. figure 11(c).

While the conclusions stated above are quite unambiguous the question arises as to whether the effects are important enough to warrant a complete overhaul of the existing constant buoyancy theories. Such a revision would, of necessity, be quite complex, and it is not clear that such an effort is required. The exponent of the head displacement history is close to that from the constant buoyancy theory, and for most purposes that description is probably quite adequate, although slightly smaller values than  $2/3$  actually give a marginally better statistical fit to the data. For a successful theory all that is needed is to have some estimate of the average buoyancy, as measured by  $(K_M/K_B)^3 B_0$ , and then the constant buoyancy theory works quite well. How one evaluates this quantity in any one case is difficult to determine. Clearly, the main effort should be in developing a good estimate of the amount of buoyant fluid that enters the head during its initial motion, as measured by Maxworthy & Nokes (2007), for example. Even this effort is a substantial one depending as it does not only on the speed and growth of the head but also the evolution of the down-slope, turbulent, stratified and unsteady feeding current, i.e. an unsteady version of the Ellison & Turner (1959) results. From table 2(a) and

for the larger locks,  $K_M$  varies over a limited range from 2.61 to 2.94, and so one might be tempted to use some mean value for each slope, as noted previously. This would certainly be an improvement over using the value  $K_B$  given by the Beghin *et al.* (1981) theory, for example. While it is certainly true that these results can be carried over to situations similar to the ones studied here, e.g. to somewhat larger channel slopes, it is unlikely that they can be used to understand situations under radically different conditions. Consider, for example, the study of currents driven by dense fluid/particle mixtures. In this case particle deposition to and erosion from an underlying bed will also be available to change the head buoyancy. There will still be buoyancy gain by a following flow and loss by shedding into a wake, but the quantitative effects will be quite different from those presented here. These effects need to be carefully evaluated to determine their effects in models that assume constant buoyancy.

The only other set of data that seems relevant to the present work is that of Rastello & Hopfinger (2004). In their figure 11 the velocity history for a lock of dimensions 20 cm  $\times$  20 cm at an angle of 32° is presented together with the appropriate version of their theory. Comparing these two and using the fact that  $U = (2/3)^{3/2} K_M^{3/2} B_0^{1/2} (x + x_0)^{-1/2}$  gives a value for  $K_M/K_B = 0.87 \pm 0.07$ , i.e.  $B/B_0 = 0.66 \pm 0.14$ . While these are somewhat larger than all of the measured values of table 2(a,b) they are certainly not unreasonably large and give support to the point of view expressed in the body of this paper.

One of the limitations of the present experiments is their restriction to relatively small slopes, as has been the case in many of the previously reported works. It is our hope to extend the effort beyond this limited range of slope when a suitable deep containment tank can be found. This would allow the determination of the values of  $B/B_0$  for larger angles than used here and check the accuracy of the estimate given above.

This work was supported internally at the Viterbi School of Engineering of the University of Southern California. The author thanks Ms Krista Gouling for her invaluable help in running the experiments that led to figures 7 and 14. Also, thanks are extended to the referees for making suggestions that greatly improved the quality of the paper.

#### REFERENCES

- ALAVIAN, V. 1986 Behavior of density currents on an incline. *J. Hydraul. Engng* **112**, 27–42.
- BEGHIN, P., HOPFINGER, E. J. & BRITTER, R. E. 1981 Gravitational convection from instantaneous sources on inclined boundaries. *J. Fluid Mech.* **107**, 407–422.
- BIRMAN, V. K., BATTANDIER, B. A., MEIBURG, E. & LINDEN, P. F. 2007 Lock-exchange flows in sloping channels. *J. Fluid Mech.* **577**, 53–77.
- BRITTER, R.E. & LINDEN, P. F. 1980 The motion of the front of a gravity current traveling down an incline. *J. Fluid Mech.* **99**, 531–543.
- CENEDESE, C. & DALZIEL, S. B. 1998 Concentration and depth fields determined by the light transmitted through a dyed solution. In *Eighth Intl. Symp. on Flow Visualization*, Sorrento, Italy.
- ELLISON, T. H. & TURNER, J. S. 1959 Turbulent entrainment in stratified flows. *J. Fluid Mech.* **6**, 423–448.
- HOPFINGER, E. J. & TOCHON-DANGUEY, J. C. 1977 A model study of powder-snow avalanches. *Glaciology* **19** (81), 343–356.
- KERSEY, D. G. & HSU, K. J. 1976 Energy relations of density-current flow: an experimental investigation. *Sedimentology* **23**, 761–789.



- LAVAL, A., CREMER, M., BEGHIN, P. & RAVENNE, C. 1988 Density surges: two-dimensional experiments. *Sedimentology* **35**, 73–84.
- LIU, Q., SCHLAPFER, D. & BUHLER, J. 1991 Motion of dense thermals on incline. *J. Hydraul. Engng* **117**, 1588–1599.
- LUTHI, S. 1991 Some new aspects of two-dimensional turbidity currents. *Sedimentology* **28**, 97–105.
- MAXWORTHY, T. & NOKES, R. I. 2007 Experiments on gravity currents propagating down slopes. Part 1. The effects of initial conditions on the release of a fixed volume of heavy fluid from an enclosed lock into an open channel. *J. Fluid Mech.* **584**, 433–453.
- RASTELLO, M. & HOPFINGER, E. J. 2004 Sediment-entraining suspension clouds: a model of powder-snow avalanches. *J. Fluid Mech.* **509**, 181–206.
- SEON, T., ZNAIEN, J., PERRIN, B., HINCH, E. J., SALIN, D. & HULIN, J. P. 2007 Front dynamics and macroscopic diffusion in buoyant mixing in tilted tubes. *Phys. Fluids* **19**, 125105.
- SIMPSON, J. E. 1987 *Gravity currents in the environment and the laboratory*, 2nd ed. Cambridge University Press.
- TICKLE, G. A. 1996 A model of the motion and dilution of a heavy gas cloud released on a uniform slope in calm conditions. *J. Haz. Mat.* **49** (1), 29–47.
- TOCHON-DANGUEY, J. C. 1977 Etude des courant de gravite sur fort pente avec application aux avalanches poudreuse. Thesis, L'Universite Scientifique et Medicale de Grenoble.
- WEBBER, D. M., JONES, S. J., & MARTIN, D. 1993 A model of the motion of a heavy gas cloud released on a uniform slope, *J. Haz Mat.* **33** (1), 101–122.